ELSEVIER

Tribology International 36 (2003) 189–197

TRIBOLOGY INTERNATIONAL

www.elsevier.com/locate/triboint

Loads carrying capacity map for the surface texture design of SiC thrust bearing sliding in water

Xiaolei Wang [a,*], Koji Kato [a], Koshi Adachi [a], Kohj Aizawa [b]

[a] *Laboratory of Tribology, School of Mechanical Engineering, Tohoku University, Sendai 980-8579, Japan*
[b] *Mechanical Engineering Research Laboratory, Hitachi, Ltd., 502, Kandatsu, Tsuchiura, Ibaraki 300-0013, Japan*

Received 7 May 2002; received in revised form 24 August 2002; accepted 4 September 2002

Abstract

Water lubricated silicon carbide is expected to be widely used for sliding bearings and mechanical seals in hydraulic systems since it is environmentally friendly and saves energy. The purpose of this study is to find the optimum surface texture to improve the load carrying capacity of SiC bearings working in water. Micro-pits, evenly distributed in a square array, were selected as the texture pattern, and formed on one of the contact surfaces by reactive ion etching. Experiments, which simulate the working condition of thrust bearings, were carried out to evaluate the effects of the micro-pits on the critical load of the transition of the lubrication mode from hydrodynamic to mixed. The results are summarized in the form of a load carrying capacity map. It was found that an optimum geometric and distributive range of micro-pits exists, where the load carrying capacity can be increased at least twice over that of an untextured surface.

Keywords: Surface texturing; Ceramic; Water; Load carrying capacity

1. Introduction

Saving energy and reducing the amount of pollution released to the environment have increasingly become very important in machine design. For sliding bearings and mechanical seals, promising combinations come from the Si-ceramics with water lubrication, which generate very low friction coefficients lower than 0.002 for Si N_4 [1] and 0.0038 for SiC [2] when they slide against themselves in water. The reason for this is that a tribo-chemical reaction occurs; the reaction product SiO_2 dissolves in water as silicic acid, which is recognized to act as a lubricant, and the contact surfaces become very smooth due to tribo-chemical wear [3–6].

These discoveries have led to the successful use of silicon carbide as the material for bearings and seals in hydraulic machines. Compared to other materials previously used, such as rubber, polytetrafluoroethylene and some soft alloys, silicon carbide not only works with very low friction, but also its wear rate remains the lowest even if the water is contaminated by sand or ferro-debris. Although the minimum friction coefficient of silicon carbide is not as low as that of silicon nitride, it maintains low friction in a much wider speed range, and its anti-seizure, anti-wear and thermal conductivity are better [7].

But along with the increase of the severity of friction contact, the problem with seizure still remains in some particular situations. Therefore, improving load carrying capacity is still an important research subject for the reliability of ceramic sliding bearings and mechanical seals.

When two parallel surfaces slide parallel to each other in the presence of a liquid, several mechanisms are recognized as reasons for the generation of hydrodynamic pressure. These include surface roughness and waviness of interfacial surfaces, squeeze, wobble and bounce, eccentric rotation, thermal and viscosity wedge etc., [8,9]. These discoveries then brought about the method of surface texturing to improve the load carrying capacity of thrust bearings and seals. Along with the development of new techniques, both its design and manufacturing method are being advanced.

* Corresponding author. Fax.: 81-22-217-6955.
E-mail address: xlwang@tribo.mech.tohoku.ac.jp (X. Wang).

0301-679X/02/$ - see front matter © 2002 Elsevier Science Ltd. All rights reserved.
PII: S0301-679X(02)00145-7

Nomenclature

a	h1/h2;
d	diameter of the pit;
C_1, C_2	constant;
h	pit depth;
h_1, h_2	film thickness;
l	interval between pits;
L, L_1	step bearing length coordinate;
P, Pm	pressure;
Q_1, Q_2	flow rate;
r	pit area ratio;
R	average radius of contact area;
s	L_1/L;
S_a	total area for contacting;
S_p	area occupied by pits;
T	friction torque;
U	average circumferential velocity;
W	load;
$\overline{W}$	dimensionless load;
W_c	critical load for the transition from hydrodynamic to mixed lubrication;
Wc_0	critical load of untextured specimens at a rotational speed of 800 rpm;
η	viscosity of lubricant;
μ	friction coefficient.

Two kinds of lubrication effects of surface textures were found in past studies.

One is the hydrodynamic effect as shown in Fig. 1 [10]. An asperity on the surface projects down into the fluid flow so as to create a step bearing. As the flow approaches the asperity, pressure increases; on the symmetrical side, the pressure decreases but not to the ideal antisymmetrical value as cavitation occurs on this side. As a result, additional load carrying capacity is generated.

Another effect acts on the condition of mixed lubrication between intimate contacting surfaces. The liquid trapped in the low region of the texture can be considered as a secondary source of lubricant, which is drawn by the relative movement to permeate into surrounding areas to reduce the friction and retard the galling. It is called the secondary lubrication effect [11].

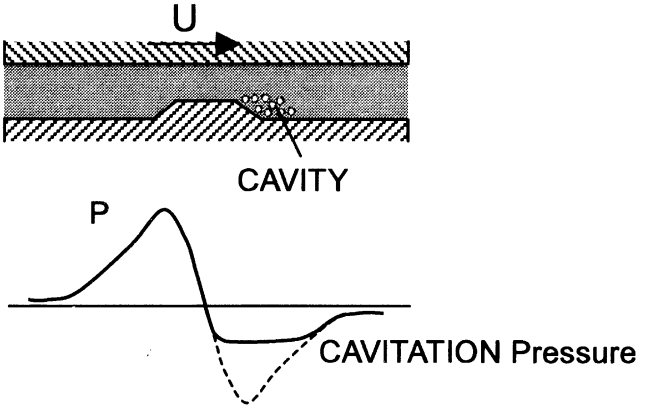

Fig. 1. The hydrodynamic effect of idealized micro asperity.

Research on the lubrication of surface textures has been carried out for a long time. Up to now, many types of surface texture including micro-islands [10,12,13], spiral grooves [14] and micro-pits [15,16] have been studied. However, analytical solutions still do not yield true and exact results when dealing with texture lubrication, although they are recognized as useful methods to explain some phenomena and to show some trends of the influences from surface textures. Especially for Si-based ceramics sliding in water, so little is known about the properties of tribo-chemical products that it is very difficult to simulate the lubrication conditions even without surface texture. Comparatively, experimentation is a realizable method that is able to provide comprehensive results on the lubrication effects of certain texture patterns.

Various manufacturing techniques are utilized to produce textures on contact surfaces. Photoetching [10] is a traditional old method which deals with the surface of copper; laser is efficient and convenient for metals; and erosion is an effective technique for hard materials.

Halperin and Etsion [16] performed an experiment on laser-textured seal rings made of steel with micro-pits (pores) of various depths to demonstrate the potential of surface texturing technology. It was found that half-

spherical pits with optimized depth can maximize the film stiffness and the PV factor at seizure inception over untextured rings by at least 150% in oil lubrication. Results from analytical solutions indicate that the effect of the pit depth over diameter ratio is more significant than that of pit area ratio (area density) [17].

Textures for nonmetal seals have also been tested. Tejima [18] formed micro-pits on the surface of SiC by micro-blasting, and carried out the friction experiments between carbon and SiC surfaces under water lubrication. It was confirmed that the minimum friction coefficient could be reduced by pits with an optimized diameter.

But the specific effects of the shape and the distribution of micro-pits are still unclear. Most previous researches concentrated only on the relationship between geometric shape and hydrodynamic pressure. However, in the situation of water lubricated self mated SiC, where tribo-chemical reaction occurs so as to make lubrication film containing reaction products together with water, the effect of micro-texture should be somewhat different than for metals lubricated with oil. Also since the lubrication film between SiC surfaces is estimated to be thinner than usual, there possibly exist some areas which lack lubricant.

Therefore, the purpose of this research is to study the effects of micro-pits on the load carrying capacity of SiC thrust bearing while tribo-chemical reaction occurs, and to find a way to show the comprehensive effects of the geometry and distribution of micro-pits.

2. Experiment

2.1. Specimens

The experiments of sliding friction were performed between the end faces of a cylinder [Fig. 2(a)] and a disk [Fig. 2(b)]. Both disk and cylinder were made of SiC, and the end faces were ground to the roughness of Rrms about 0.2 μm.

The end face of the disk was then textured with round micro-pits arranged in a square array as shown in Fig. 2 by the way of reactive ion etching (RIE) using a mask. Since the material is etched mainly in the direction of ion movement, the pits were formed in the shape of cylinder as shown in Fig. 3. The roughness of the pit bottom was related to the roughness of the original surface before etching and the anisotropic etching property of SiC material. The diameter and arrangement of the pits was determined by a metal mask formed on surface. The depth of pits was controlled by the etching time. The intervals between pits were changed to obtain a series of different pit area ratios.

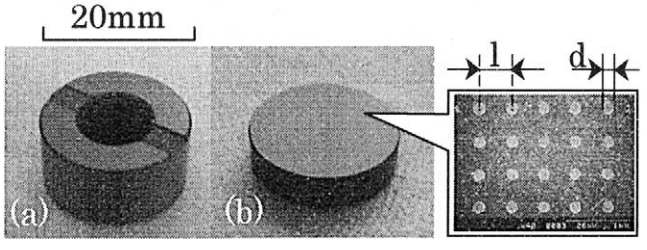

Fig. 2. The Appearance of the specimens, (a) cylinder, (b) disk.

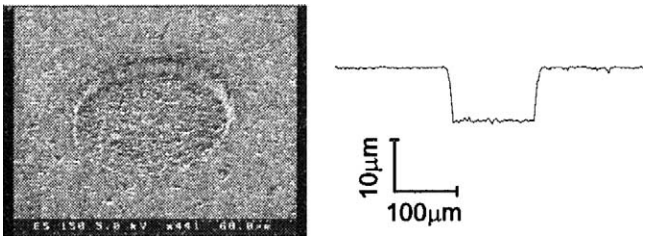

Fig. 3. The SEM photo and cross profile of a micro-pit produced by RIE.

$$r = \frac{S_p}{S_a} = \frac{\pi d^2}{4l^2},\%.$$

All cylinders (Fig. 2(a)) were the same, with a hole in the center, and two grooves on the end surface to allow the water to be supplied to the contact surfaces. The purpose of this design is to simulate the contact condition of sliding thrust bearings.

Table 1 shows the disks used in this study. They have pits with diameters ranging from 50 to 650 μm, depths from 2.0 to 16.6 μm, and pit area ratios from 0 to 22.5%.

2.2. Apparatus

Fig. 4 shows the apparatus used in this experiment.

The cylinder is mated to the disk and driven by a motor with an adjustable rotational speed. The disk is supported by a half-spherical tip so that its friction surface is automatically aligned to match the surface of the cylinder. Load is applied by a hydraulic system from the bottom of disk. Purified water is supplied by a volume-controllable pump to the center of the cylinder, via the

Table 1
Geometrical parameters of disks

No.	Pit diameter d (μm)	Pit depth h (μm)	Pit interval l (μm)	Pit area ratio r (%)
1	0	0	0	0
2	50	3.2	200	5.0
3	150	2.0–13.2	800–280	2.8–22.5
4	250	2.4–16.6	1330–470	2.8–22.5
5	350	3.2	1870–650	2.8–22.5
6	500	3.4	2670–930	2.8–22.5
7	650	3.3	2600	5.0

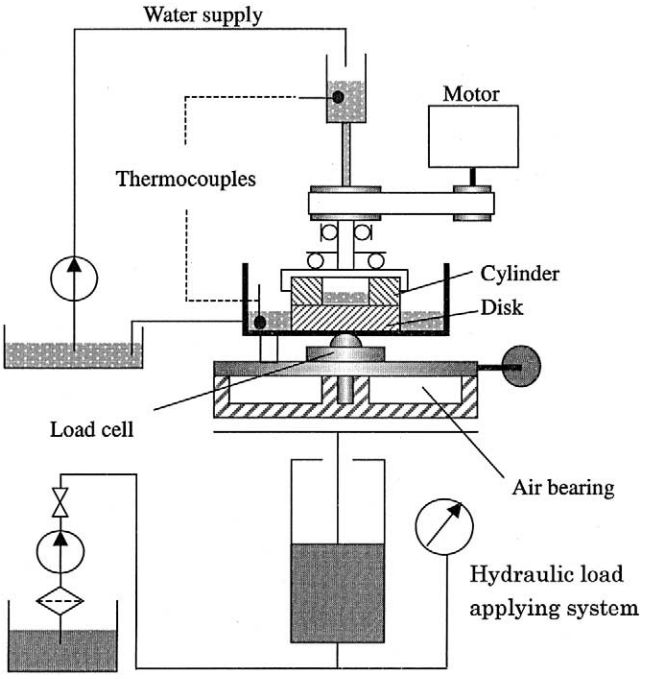

Fig. 4. Schematic diagram of experimental apparatus.

grooves to the friction surfaces. Water is used only once to avoid the influence of wear debris and the change of electrical conductivity. The temperature of the water at the inlet and the outlet is monitored by thermocouples. Load and friction torque are detected by the load cells. An air bearing is used to support the disk so that very small friction torque (< 0.001 Nm) can be detected accurately.

An auto-stop system is used to stop the load applying system and the driving motor to avoid damage to apparatus and specimens when the friction torque rises suddenly.

The testing conditions are listed in Table 2. The temperature of the water supplied to the friction surfaces was accurately controlled since past studies showed that temperature has a large effect on friction [19].

2.3. Test procedure

Previous work has shown that surface roughness plays an important role in friction and lubrication of SiC since the thickness of the lubrication film is estimated to be very thin [20]. Also inappropriate polishing often causes flatness degradation which is important for the generation of lubrication film. So before the test all the specimens had the same running-in procedure as shown in Fig. 5, which was performed at a rotational speed of 1000 rpm. When the load was increased, the friction torque jumped to a higher level and then slowly decreased. This means that the contact and lubrication conditions were improved through wear. The rate that the friction torque decreases can be regarded as the rate of running in. So after the friction torque no longer decreased, a greater load was applied. This step was repeated in increments of about 100 N at a time until the friction torque no longer fell and reached the upper limit of the load cell. This means that even under greater load, further running-in could not be conducted in this situation.

Through running in, the surface around the pits was worn and became smooth. Thereafter, the friction tests under various loads and speeds were performed. The friction coefficient was calculated as follows.

$$\mu = \frac{T}{WR}.$$

Table 2
Experimental conditions

Load:	300–3000 N
Contact pressure:	1.5–15 MPa
Rotational speed:	400–1200 rpm
Sliding speed:	0.31–0.94 m/s
Lubricant:	Purified water
Supply rate:	60 ml/min
Temperature:	17–19 °C
Humidity:	40–60%

2.4. Results

Fig. 6 shows typical trends of the friction coefficient for SiC sliding in water. The common feature of these three curves is that the friction coefficient remains at a very low level while the load is light, and when the load exceeds a certain value, the friction suddenly rises. Although the value of friction coefficient is still low (< 0.1) at this time, but if the load was increased continually, seizure would occur.

The figure shows that friction properties are influenced by the pit area ratio. The low friction range becomes wider with the increase of the pit area ratio from 2.8 to 4.9%, but rapidly decreases when pit area ratio reaches 22.5%. This implies that there should exist an optimum value for the pit area ratio which could max-

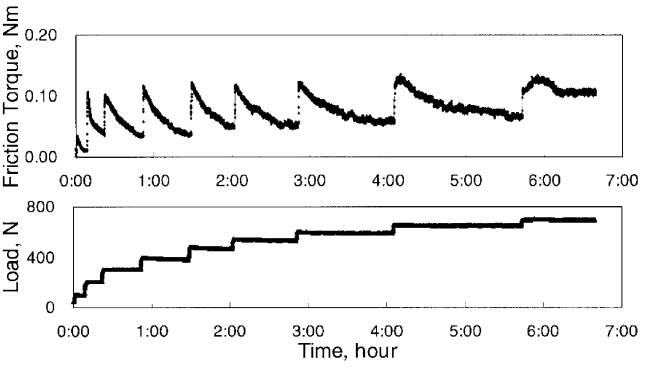

Fig. 5. The running-in process.

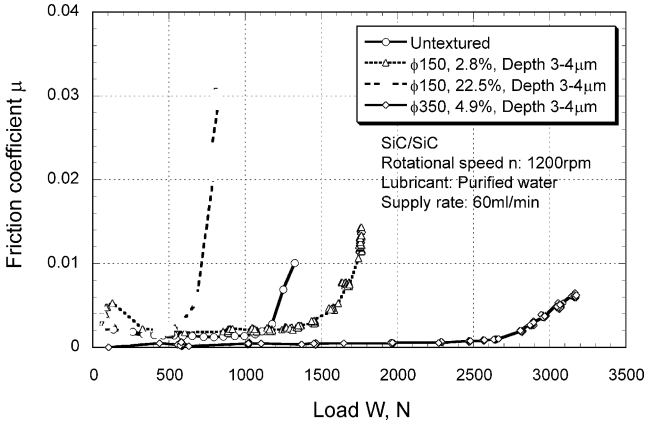

Fig. 6. Friction coefficient m versus load W for SiC cylinder/SiC textured disk in water at rotational speed of 1200rpm.

imize the low friction range of SiC sliding in water. Similar results were also obtained from experiments dealing with the effects of the pit depth and the pit diameter.

Fig. 7 shows a typical Stribeck curve of SiC sliding in water. The fact that the low friction range exists and its value is very low, approximately 0.001–0.003, suggests it is in the state of hydrodynamic lubrication. Thus, the sudden increase of friction coefficient from a stable low value can be considered as the transition of the lubrication mode from hydrodynamic to mixed.

Therefore, the load at which the friction coefficient starts its sudden increase (Figs. 6 and 7), is defined as the critical load Wc for the transition from hydrodynamic to mixed lubrication so as to evaluate the effects of the surface texture in this experiment. A high critical load means the hydrodynamic lubrication region is large, and the load carrying capacity is great.

Figs. 8–10 are examples of the effects of the pit depth, pit area ratio and the pit diameter on the critical load. They are summarized from the results of basic friction

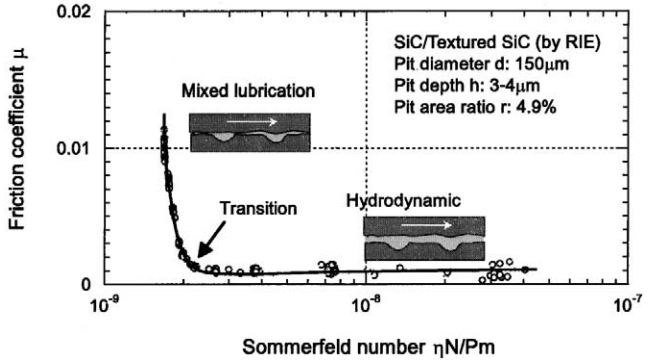

Fig. 7. Stribeck curve of SiC cylinder/SiC textured disk in water

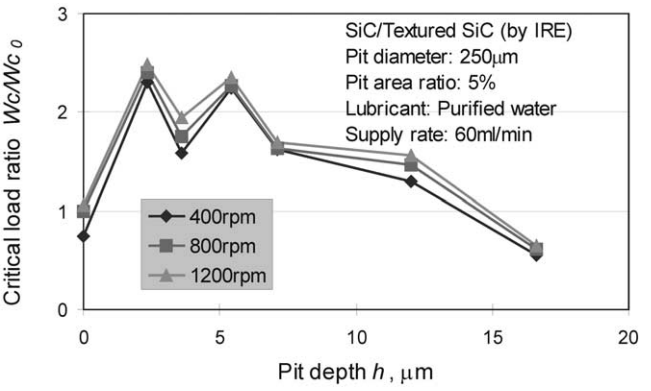

Fig. 8. The effect of the pit depth.

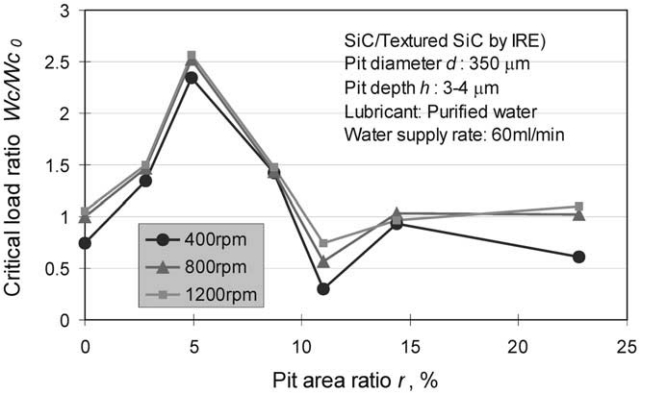

Fig. 9. The effect of the pit area ratio.

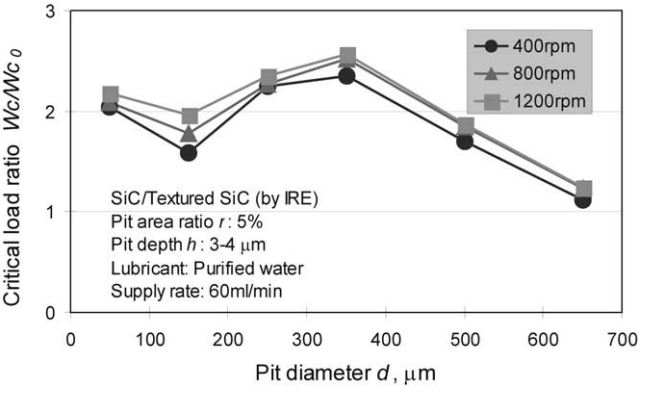

Fig. 10. The effect of the pit diameter.

tests as shown in Fig. 6. In order to show the effect of surface texture clearly, the graphs were drawn in the form of critical load ratio Wc/Wc_0, where Wc stands for the critical load of textured specimen, and Wc_0 stands for the critical load of untextured specimen at a rotational speed of 800 rpm.

The three curves in each graph were obtained at three different rotational speeds; 400, 800 and 1200 rpm. Gen-

erally, a high rotational speed leads to a high critical load although the difference is not large.

For the effects of the pit depth as shown in Fig. 8, there is an obvious increase of the critical load Wc in depths ranging from 3 to 6 μm. It seems that shallow pits could possibly result in a high critical load. But the test of pit depth shallower than 2 μm was not carried out in this experiment due to the etching time becoming so short that the stability of the plasma was difficult to control. The maximum value of the critical load was obtained with a pit depth about 2 μm; it was near 2.5 times that of an untextured surface.

Fig. 9 shows the effects of the pit area ratio on the critical load Wc at rotational speeds of 400, 800 and 1200 rpm. In the pit area ratio range of 0–10%, the critical load is increased by surface texture. The disk with the pit area ratio of 5% in this experiment gave the best results: an increase of nearly 2.5 times in critical load over that of an untextured specimen. When the pit area ratio exceeds 10%, the critical load Wc decreases to a value near that of an untextured one, therefore, it does not provide any improvement to the load carrying capacity.

Fig. 10 shows the effects of the pit diameter on the critical load Wc at rotational speeds of 400, 800 and 1200 rpm. The pit area ratio is 5% and the pit depth is in the range of 3–4 μm. The critical load of the specimen with a diameter of 150 μm does not exceed a value two times over that of untextured specimen. The specimens with pit diameters of 250 and 350 μm gave better results in this condition. Both of their critical loads increased more than 2 times, and that of the specimen with a pit diameter of 350 μm is near 2.5 times over that of an untextured surface.

These results remind us that the effects of the pit depth, diameter and the pit area ratio should be considered comprehensively for the purpose of maximizing the critical load. In other words, graphs demonstrating the optimum combinations of pit geometry and distribution are needed.

Fig. 11 is an attempt to summarize the effects of the pit depth and diameter into one graph. The horizontal axis represents the depth-diameter ratio h/d and the vertical axis is the critical load ratio. The distribution of most experimental data shows a definite trend of the critical load ratio Wc/Wc_0 versus the depth-diameter ratio h/d. Thus, it suggests that this summarizing method is suitable for the data obtained in this experiment.

Therefore, a load carrying capacity map for textured SiC sliding in water is drawn in Fig. 12. On the horizontal axis, the depth-diameter ratio h/d describes the geometry of the pit. On the vertical axis, the pit area ratio *r* describes the distribution density of the pits on the contact surface. For the conditions marked with '●', the critical load is increased at least 2 times over that of an untextured surface; for '◍' and ' ', the increases are between 1.5–2.0 times and 1.0–1.5 times respectively; and for conditions marked with '○', the critical load is decreased. It is now clear that there exists a region around the pit area ratio of 5% and depth-diameter ratio of 0.015, where critical load is increased at least twice over that of the untextured specimen.

3. Discussion

A theoretical analysis was performed to determine the feasibility of the lubrication mechanism suggested by experimental results. Because of the complexity of the free boundary problem associated with cavitation, as well as the interaction between pits, several assumptions were made, and the results of the theoretical analysis are expected to show only the trends of the effects of the pit depth, diameter and the pit area ratio.

The problem has been simplified to two dimensions as shown in Fig. 13. Each pit is assumed to be antisymmetric, that is, the pressure increases on one side and decreases on the opposite side. Since cavitation will be

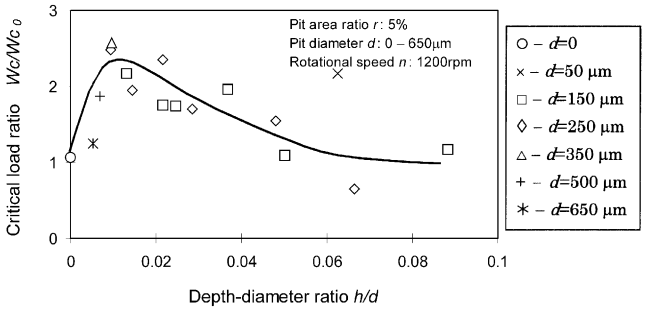

Fig. 11. The critical load ratio Wc/Wc_0 versus depth-diameter ratio h/d.

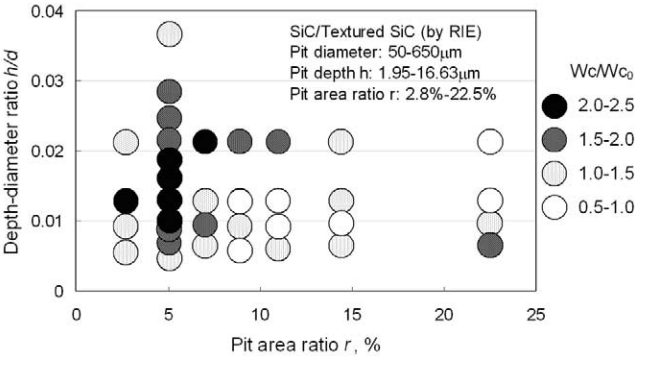

Fig. 12. The Load carrying capacity map of SiC thrust bearings in water.

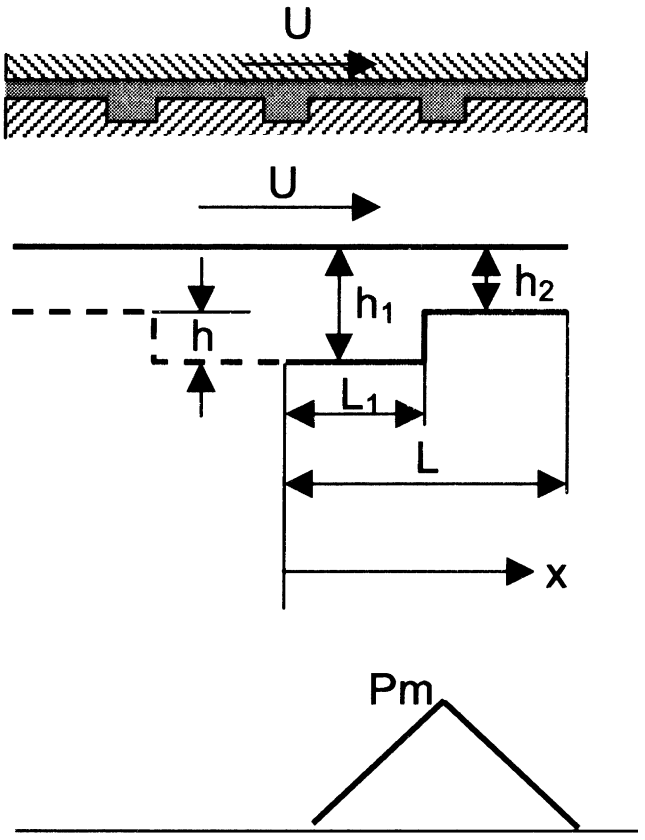

Fig. 13. The pit geometry.

generated when the pressure decreases below the cavitation pressure, the pressure of the negative side is replaced by the cavitation pressure, which is simplified to 0 in this study. Therefore, only the side with positive pressure needs to be calculated. This side could be considered as a step bearing. Additionally, the pressure at the midpoint between the two pits was also assumed to be 0. This means that short intervals between pits would result in a rapid decrease of the hydrodynamic pressure.

Since the film thickness is constant both in inlet region ($0 \le x \le L_1$)y and outlet region ($L_1 \le x \le L$), the Reynolds equation is simplified to

$$\frac{d^2p}{dx^2} = 0,$$

$$p = C_1x + C_2.$$

This equation is solved separately for the two regions from the boundary conditions:

$$p = 0 \text{ for } x = 0 \quad p = Pm \text{ for } x = L_1 \quad p = 0 \text{ for } x = L,$$

where P_m is the unknown pressure existing at the discontinuity.

Thus, the pressure distribution in inlet region is

$$p = \frac{P_m}{L_1}x$$

and in outlet region is

$$p = \frac{P_m}{(L-L_1)}(L-x).$$

These resemble a triangle as shown in Fig. 13. Then, by equating the rates of flow Q_1 in inlet region and Q_2 in outlet region, where

$$Q_i = -\frac{h_i^3}{12\eta}\frac{dp_i}{dx} + \frac{Uh_i}{2} \qquad i = 1,2$$

the maximum pressure occurs at the step is given by

$$Pm = \frac{6\eta UL}{h_2^2} \bullet \frac{s(1-s)(a-1)}{a^3(1-s) + s}$$

where $a = h_1/h_2$, $s = L_1/L$ [21].

Therefore, the total load in two dimensions, which can be supported by this pit, is given by:

$$W = L\frac{Pm}{2} = \frac{3\eta UL^2}{h_2^2} \bullet \frac{s(1-s)(a-1)}{a^3(1-s) + s}$$

which includes two main parts, the left part includes operating conditions (η, U) and given conditions (h_2, L), the right part are geometry and distribution conditions of pit pattern. Therefore, the right part is defined as a dimensionless load that express the effects of the pit geometry and distribution as shown below.

$$\bar{W} = \frac{s(1-s)(a-1)}{a^3(1-s) + s}.$$

In order to compare the results between the theoretical analysis and experiments, the dimensionless load was calculated and plotted in Fig. 14 on the same x and y axis as Fig. 12.

It is clear that the results of the theoretical analysis represent similar trends to those of the experimental data. This indicates that the hydrodynamic effects play the leading role in the micro-pits lubrication under these experimental conditions, and the existence of optimum geometry and distribution range for the critical load is reasonable.

For the geometry and distribution values of micro-pits which maximize the critical load, there are large differences between the results of experiment and calculation. The optimum value of the pit area ratio found through the calculation is larger than 40%, while that of the experiment was around 5%. This might be because the increase of the contact pressure, as a direct result of the decrease of the contact area, was not considered in the theoretical calculations. For the difference of the depth-diameter ratio between calculation and experiment, experimental results indicate that deeper pits than the optimal calculated value result in a higher critical load.

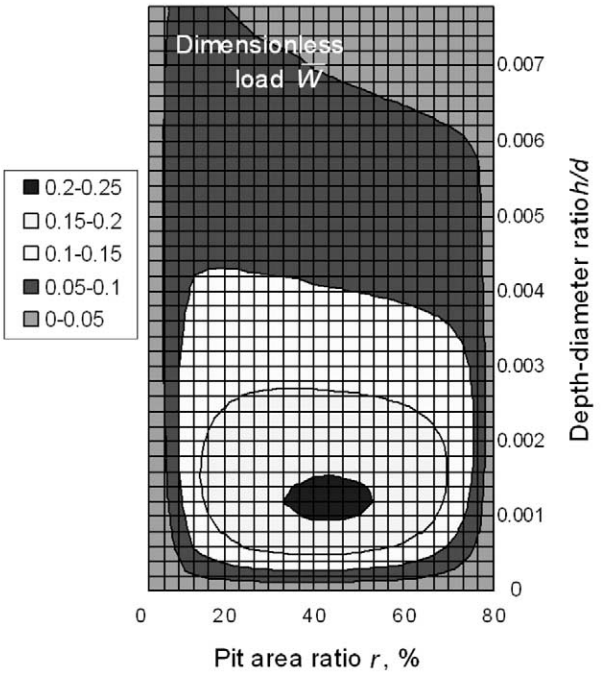

Fig. 14. Theoretical effect of pit area ratio r and depth-diameter meter ratio h/d on the dimensionless load $\bar{W}$.

Beside the errors due to the assumptions which are necessary to simplify the theoretical problem of hydrodynamic pressure, another possible reason is that deeper pits are better for storing water, which should be driven to the contact region by the moving surface and capillarity effect during sliding. This is not only helpful to reduce the high friction resulted by lack of lubricant in some area, but also capable of keeping the reaction of tribo-chemistry, which is supposed to generate a film of reaction products on the contact surfaces to keep low friction.

4. Conclusions

In order to increase the load carrying capacity of SiC thrust bearing in water lubrication, micro-pits were introduced on one contact surface by reactive ion etching (RIE). The pits effects on the critical load for the transition from hydrodynamic to mixed lubrication were studied experimentally. It was found that micro-pit texturing is an effective way to raise the load carrying capacity of SiC thrust bearings in water lubrication, where a tribo-chemical reaction occurs. Depending on the geometry and distribution of the micro-pits, the load carrying capacity, measured by the critical load was improved up to about 2.5 times over that of untextured surface. The following conclusions have been drawn as the most significant:

1. A load carrying capacity map, which shows the relationship between the increments of the critical load and pit conditions, was developed for the purpose of micro-pit design.
2. There exists an optimum range for the pit geometry factor, depth-diameter ratio h/d, and the distribution factor, pit area ratio *r*, where the critical load can be improved at least twice over that of an untextured surface.
3. The maximum increment of critical load in this experiment was about 2.5 times that of an untextured one, which was obtained for pit conditions with the diameter at 350 μm, the depth at 3.2 μm and the pit area ratio at 5%.
4. The possibility that such optimum geometry and distribution range of the micro-pits exists was qualitatively verified by a theoretical analysis.

References

[1] Tomizawa H, Fischer TE. Friction and wear of silicon nitride and silicon carbide in water: Hydrodynamic lubrication at low sliding speed obtained by tribochemical wear. ASLE Trans 1987;30(1):41–6.
[2] Wong HC, Umehara N, Kato K. Frictional characteristics of ceramics under water-lubricated conditions. Tribology Letters 1998;5(4):303–8.
[3] Sugita T, Ueda K, Kanemura Y. Material removal mechanism of silicon nitride during rubbing in water. Wear 1984;97:1–8.
[4] Ishigaki H, Nagata R, Iwasa M. Effect of adsorbed water on friction of hot-pressed silicon nitride and silicon carbide at low speed sliding. Wear 1988;121:107–16.
[5] Saito T, Imada Y, Honda F. An analytical observation of the tribochemical reaction of silicon nitride sliding with low friction in aqueous solutions. Wear 1997;205:153–9.
[6] Hsu SM, Shen MC. Ceramic wear maps. Wear 1996;200:154–75.
[7] Nau BS. Mechanical seal face materials. Proceedings of the Institution of Mechanical Engineers 1997;211(J):165–83.
[8] Ludwig LP, Greiner HF. Designing mechanical face seals for improved performance Part 2—Lubrication. Mechanical Engineering 1978;100(12):18–23.
[9] Lebeck AO. Parallel sliding load support in the mixed friction regime. Part 2—Evaluation of the mechanisms. Trans ASME, Journal of Tribology 1987;109(1):196–205.
[10] Hamilton DB, Walowit JA, Allen CM. A theory of lubrication by micro-irregularities. Trans ASME, Journal of Basic Engineering 1966;88(1):177–85.
[11] Lo SW, Horng TC. Lubricant permeation from micro oil pits under intimate contact condition. Trans ASME, Journal of Tribology 1999;121(10):633–8.
[12] Anno JN, Walowit JA, Allen CM. Microasperity lubrication. Journal of Lubrication Technology 1968;4:351–5.
[13] Anno JN, Walowit JA, Allen CM. Load support and leakage from microasperity-lubricated face seal. Trans ASME, Journal of Lubrication Technology 1969;10:726–31.
[14] Lai T. Development of non-contacting, non-leaking spiral groove liquid face seals. Lubrication Engineering 1994;8:625–31.
[15] Geiger M, Roth S, Becker W. Influence of laser-produced microstructures on the tribological behaviour of ceramics. Surface and Coatings Technology 1998;101(1-3):17–22.
[16] Halperin G, Greenberg Y, Etsion I. Increasing mechanical seal life with laser-textured seal faces. In: Proceedings of the 15th

International Conf. on Fluid Sealing, 1997. Maastricht: BHR Group; 1997. p. 3–11.
[17] Etsion I, Kligerman Y, Halperin G. Analytical and experimental investigation of laser-textured mechanical seal faces. Tribology Transactions 1999;42(3):511–6.
[18] Tejima Y, Ishiyama S, Ura A. The influence of pores at sliding faces and the pores diameter on mechanical seals performance. Journal of Japanese Society of Tribologists 1999;44(6):54–61.
[19] Xu J, Kato K, Hirayama T. The transition of wear mode during the running-in process of silicon nitride sliding in water. Wear 1997;205:55–63.
[20] Wong HC, Umehara N, Kato K. The effect of surface roughness on friction of ceramics sliding in water. Wear 1998;218(2):237–43.
[21] Dowson D, editor. Hydrodynamic lubrication bearings and thrust bearings. Elsevier; 1997.